Extraction of the materials parameters that determine the mobility in disordered organic semiconductors from the current-voltage characteristics: Accuracy and limitations

R. J. de Vries,[1,2,3] A. Badinski,[4] R. A. J. Janssen,[2] and R. Coehoorn[2,3,a)]
[1]*Dutch Polymer Institute (DPI), P.O. Box 902, 5600 AX Eindhoven, The Netherlands*
[2]*Molecular Materials and Nanosystems, Department of Applied Physics, Eindhoven University of Technology, P.O. Box 513, 5600 MB Eindhoven, The Netherlands*
[3]*Philips Research Laboratories, High Tech Campus 4, 5656 AE Eindhoven, The Netherlands*
[4]*BASF SE, GVM/S—B009, 67056 Ludwigshafen, Germany*

(Received 9 December 2012; accepted 2 March 2013; published online 19 March 2013)

The development and application of predictive models for organic electronic devices with a complex layer structure, such as white organic light-emitting diodes, require the availability of an accurate and fast method for extracting the materials parameters, which determine the mobility in each of the layers from a set of experimental data. The absence of such a generally used method may be regarded as one of the reasons why so far relatively little consensus has been obtained concerning the most appropriate transport model, the shape of the density of states (DOS), and the underlying microscopic parameters, such as the width of the DOS and the density of hopping sites. In this paper, we present a time-efficient Gauss-Newton method for extracting these parameters from current-voltage curves for single-carrier devices, obtained for various layer thicknesses and temperatures. The method takes the experimental uncertainties into account and provides the correlated uncertainty margins of the parameters studied. We focus on materials with a Gaussian DOS with random and spatially correlated disorder. Making use of artificially generated as well as experimental data sets, we demonstrate the accuracy and limitations, and show that it is possible to deduce the type of disorder from the analysis. The presence of an exponential trap DOS, as is often observed for the case of electron transport, is found to significantly reduce the accuracy of the transport parameters obtained. © *2013 American Institute of Physics*.
[http://dx.doi.org/10.1063/1.4795588]

I. INTRODUCTION

In the past decade, strong progress has been made concerning the description of charge transport processes in disordered organic semiconductors.[1,2] In particular, enhanced understanding has been obtained of the charge carrier density dependence of the mobility resulting from energetic disorder. Experimental proof of the carrier density dependence of the mobility was obtained from the current density (J) versus voltage (V) characteristics of organic field effect transistors (OFETs) and from the $J(V)$ characteristics of sandwich-type devices as used in organic light-emitting diodes (OLEDs).[3–5]

Whereas the $J(V)$ curves of OFETs based on materials with a disordered structure can often be consistently described assuming an exponential density of states (DOS),[3,4] the shape of the hole-only $J(V)$ characteristics of sandwich-type devices based on polymers used in OLEDs is often better described using a Gaussian DOS.[6–9] In a Gaussian DOS, the charge carriers act at low carrier concentrations, in the so-called Boltzmann regime, as independent particles. The mobility is then constant. Above a critical carrier concentration, the mobility increases with increasing charge carrier density as low-energy states, which would otherwise act as traps are then already filled.[10–14] For the case of a Gaussian DOS with spatially random site energies, Pasveer *et al*. obtained accurate expressions for the temperature (T), electric field (F), and charge carrier density (n) dependence of the mobility from three-dimensional modelling ("extended Gaussian disorder model," EGDM).[6] An analogous approach for the case of a Gaussian DOS with spatially correlated site energies, by Bouhassoune *et al*., led to the "extended Correlated disorder model" (ECDM).[15] Within the ECDM, the field dependence of the mobility is much stronger than in the EGDM, but the carrier density dependence is somewhat smaller. When using sandwich-type single-carrier devices, a clear distinction may be made with the conventionally used mobility model,[17,18] within which the carrier density dependence is neglected and within which an empirical Poole-Frenkel type ($\ln(\mu) \propto F$) dependence of the mobility (μ) on the electric field (F) is assumed, viz. by carrying out $J(V)$ curve measurements for various layer thicknesses.[16]

Being able to make a distinction between various models, to determine the type of disorder and to accurately extract the materials parameters that determine the mobility in disordered organic semiconductors is of great importance to the rational design of OLEDs, in particular when multilayer stacks are used. The shape of the DOS and the type of disorder (random or spatially correlated) are in general not known *a priori*. Only recently, the feasibility of obtaining such information

a)reinder.coehoorn@philips.com

from first-principles theoretical studies of the molecular and energetic structure of organic semiconductors has been demonstrated, combining molecular dynamics modeling and density functional theory.[19–23] Analyses of measured $J(V)$ curves of sandwich-type devices have been successfully carried out using the EGDM for several polymers,[8,24–27] whereas for several small-molecule materials, a more consistent analysis was obtained using the ECDM.[28,29] However, in these studies, no systematic method was applied for obtaining quantified uncertainty margins of the parameters studied and their possible correlations. Furthermore, it has remained unclear to what extent it is possible to make a distinction between different mobility models, e.g., the EGDM and the ECDM.

In this paper, we investigate these issues in a systematic manner by carrying out a study of the accuracy and limitations of a parameter extraction method based on a Gauss-Newton algorithm.[30–32] Within the method developed, the optimal set of parameter values follows iteratively from a least-squares fit of the measured current density as calculated assuming a linear sensitivity to a change of the parameter values, around a trial set of parameter values. The algorithm is thus most efficient if the quantity to be analyzed varies approximately linearly with each of the parameter values. In order to more closely achieve this situation, we have chosen to apply the method to the measured $\log_{10}(J(V))$ curves, instead of the $J(V)$ curves. The method includes the influence of the experimental uncertainty in the measured current density and provides a covariance matrix which expresses the correlated uncertainties of all parameters. We note that it is not known whether, in realistic cases, the linearization assumption is valid to a sufficient extent, so that the predicted ellipsoidal confidence regions obtained surrounding the optimal point in parameter space coincide sufficiently well to the confidence regions that would follow from a (time-consuming) brute force approach within which the merit function is calculated explicitly for a dense grid of parameter values surrounding the optimal point. Furthermore, it is not *a priori* clear whether, in all cases, a unique solution, which is essentially independent of the starting conditions, is found. Indeed, we will show that a unique solution exists often, but not in all cases.

In order to investigate the strengths and limitations of the method used, we study a series of cases with increasing complexity of the problem to be solved, i.e., with an increasing number of parameters. In all cases, single-layer systems are studied with an energy level structure, such as shown in Figure 1, but with values of the injection barriers such that the transport is unipolar. The transport takes place by hopping of either holes or electrons in between energetically random or spatially correlated states with a Gaussian energy distribution. The mobility is then given by the EGDM and the ECDM, respectively, in which the only materials parameters are the width of the DOS, σ, the total hopping site density, N_t, and the (temperature dependent) mobility in the limit of zero field and zero carrier density, μ_0. The total hopping site density determines the average hopping site distance, a, which is defined as $a \equiv N_t^{1/3}$. In our analyses, we include a study of the effects of injection barriers (Δ) for holes (h) and electrons (e) at the anode (A) and cathode (C). The built-in voltage V_{bi} is equal to $\Delta_{C,h} - \Delta_{A,h}$ and $\Delta_{A,e} - \Delta_{C,e}$ for the case of hole and electron-only devices, respectively. Furthermore, we study the effect of the presence of a superimposed exponential trap density of states, as is often assumed for the case of electron transport.[26,34,35] The total DOS is then described using two additional parameters, viz. the total density of trap states $N_{t,trap}$ and the characteristic $1/e$ decay energy of the trap DOS, E_0. We first explore the performance of the method by studying two examples based on artificial noise-containing datasets. It is shown how in an efficient manner a unique solution is found, how a clear distinction can be made between the EGDM and the ECDM, and how as a result of the increasing complexity (more model parameters) of the problem studied the uncertainty region increases when including trap states. We show how this uncertainty can be reduced by making use of available experimental information on one of the parameters, and argue that, in particular when studying electron-transport, this will often be necessary in order to obtain the parameter values with sufficient accuracy. Subsequently, the method is applied to the case of experimental $J(V)$ curves as measured for hole-only[8] and electron-only[26] devices based on a blue-emitting polyfluorene-triarylamine copolymer (PF-TAA), and a comparison is made with earlier published analyzes. Table I gives an overview of the four cases studied.

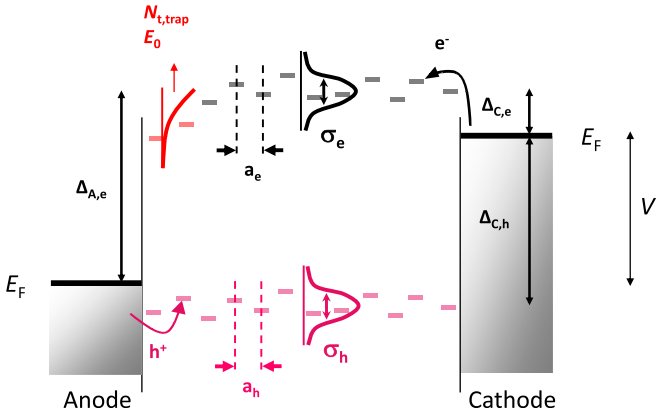

FIG. 1. Schematic energy level diagram of a double-carrier device indicating all materials and device parameters included in this study. For holes (h^+) and electrons (e^-), the widths of the DOS, $\sigma_{e,h}$, the hopping site distances $a_{e,h}$, and the injection barriers Δ at the anode (A) and cathode (C) are indicated. For the electrons, the superimposed exponential DOS is indicated with the two additional parameters involved, E_0 and $N_{t,trap}$. An applied voltage (V) leads to an energy difference between the Fermi levels (E_F) of the anode and the cathode.

In Sec. II, the method is presented. Section III contains the application to the two artificial datasets, and in Sec. IV, the method is applied to the hole and electron transport in PF-TAA. Section V contains a summary and conclusions.

II. METHOD

Within the Gauss-Newton method used, the set of n experimental current densities $J_{exp,i}$ as obtained at various device thicknesses and measurement conditions is analyzed using a set $P \equiv \{P_1, P_2, ..., P_m\}$ of m parameter values describing the transport. These parameters are chosen to be obtained by minimizing a χ^2 merit function, which is here defined as

TABLE I. Overview of the cases studied in this paper. The description indicates which of the elements, shown in Figure 1, are included. A = artificial data and E = experimental data.

Section	Data	Description
III A	A	No traps, ideal injecting contact, finite V_{bi}, and EGDM and ECDM analysis.
III B	A	Exponential trap DOS, ideal injecting contact, finite V_{bi}, and ECDM analysis.
IV A	E	No traps, ideal contacts, and EGDM and ECDM analysis.
IV B	E	Exponential trap DOS, injection barriers at both electrodes, and EGDM analysis.

$$\chi^2(P) \equiv \frac{1}{n}\sum_{i=1}^{n}\frac{[\log_{10}(J_{\text{model,P,i}}) - \log_{10}(J_{\text{exp,i}})]^2}{\alpha_i^2}, \equiv \frac{1}{n}\sum_{i=1}^{n}(F_i(P))^2. \quad (1)$$

In this expression, $\log_{10}(J_{\text{model,P,i}})$ is the logarithm of the predicted current density, and α_i is the standard deviation of the logarithm of the measured current density, in both cases for the *i*th experiment. Choosing the logarithm of the current density as the observable is found to provide a quite linear variation of the observable with the parameters to be determined. The experimental uncertainty in the observable is assumed to be normally distributed. For the same reason, we have chosen the logarithms of N_t, $N_{t,trap}$, and of μ_0 as the parameters to be determined. In practice, the experimental data points are obtained by varying for a given type of device, the voltage, layer thickness L, and temperature T.

Minimizing $\chi^2(P)$ is an iterative procedure. First, for the previously determined "old" parameter set, the partial derivatives of J with respect to the value of each of the parameters are calculated. Subsequently, the partial derivatives of F are obtained, and a Taylor expansion of $\chi^2(P)$ of the form

$$\chi^2_{\text{new}} = \min_{P_{j,\text{new}}}\left\{\frac{1}{n}\sum_{i=1}^{n}\left[F_i(P_{\text{old}}) + \sum_{j=1}^{m}\frac{\partial F_i}{\partial P_j}(P_{j,\text{new}} - P_{j,\text{old}})\right]^2\right\}, \quad (2)$$

is used to predict the optimal change $(P_{j,\text{new}} - P_{j,\text{old}})$ of each of the parameters ($j = 1, 2, \ldots, m$), leading by minimization to a new prediction for χ^2. This procedure is iterated until convergence is reached.

It is not *a priori* clear whether the approach described above will give rise to a unique solution in all cases. It cannot be excluded that the function $\chi^2(P)$ shows multiple local minima, e.g., as a result of the experimental uncertainties, as a result of the use of an insufficiently rich experimental data set, or as a result of the use of an incorrect transport model. We will investigate this explicitly for several cases by repeating the iterative procedure after starting at different initial points in the parameter space. Furthermore, it is not in all cases *a priori* clear whether the model used will actually provide a good description of the transport process in the material investigated. One may expect that the final "observed" value for the merit function, $\chi 2_{\text{obs}}$, is then significantly larger than the statistically expected value. In order to investigate this, one may carry out a so-called "χ^2-test,"[32] making use of the probability density function of the χ^2 distribution

$$f_{\chi^2}(x) = \frac{1}{2^{\nu/2}\Gamma(\nu/2)}x^{\frac{1}{2}\nu - 1}e^{-x/2}, \quad (3)$$

where $\nu = n - m$. If the mathematical model used is correct and if the experimental errors are normally distributed and correctly estimated, the value of the parameter,

$$p = \int_{\chi^2_{obs}}^{\infty} f_{\chi^2}(x)dx, \quad (4)$$

is expected to be uniformly distributed between 0 and 1. The finding of a value of p very close to 1 would provide an indication that the model used is incorrect or incomplete. The finding of a very small value of p, close to 0, might indicate that the experimental errors have been overestimated. The χ^2-test thus provides a tool for validating a certain transport model.

The uncertainty margins in the parameters are fully quantified by the covariance matrix C, defined as

$$C = (A^T \cdot A)^{-1} \quad (5)$$

with $A \equiv (\partial F_i/\partial P_k)$. The diagonal elements C_{jj} are equal to the square of the standard deviation of the parameter P_j. In this paper, the 95% confidence intervals are given for the normal distribution assumed. The half-width is then equal to $1.96 \cdot C_{jj}^{1/2}$.

Often, correlations between the parameters are significant. Their pairwise correlation is expressed by the correlation matrix. The matrix elements are defined as $\rho_{ij} \equiv C_{ij}/\sqrt{C_{ii} \cdot C_{jj}}$, a number in between -1 and $+1$. The standard deviations provide only the widths of the probability distributions for each single parameter. They take the complexity of the problem, within which the parameter values may be correlated, into account, but they do not yet provide the *joint* m-dimensional probability distribution, which would be needed to make a prediction of the uncertainty of the predicted current density in a device. In this joint probability distribution, the contours of equal probability density (expressed in terms of dimensionless units, i.e., by expressing the parameter values in units of the standard deviation) are m-dimensional ellipsoids centered around the optimal point.[32] These ellipsoids enclose joint uncertainty regions, corresponding to a certain level of confidence.

In this paper, we show as an example for the case of an artificial dataset the 95% confidence ellipsoid around the selected parameter value point P, containing with a 95% probability the outcome of the extraction procedure if noise is included (see Sec. III A). It may be obtained from the covariance matrix using

$$UC^{-1}U^{T} = \Delta_m^2, \tag{6}$$

where U is the vector $(u_1, u_2, ..., u_m)$, with u_j the deviation of the jth parameter from the optimal value (i.e., the value at which convergence is reached), and where Δ_m^2 is the 95th percentile of the χ^2-distribution with m degrees of freedom. The half-widths of the projection of these 95% confidence ellipsoids on the P_j axes are equal to $\Delta_m \cdot C_{jj}^{1/2}$. The value of Δ_1 is equal to 1.96, and Δ_m increases with increasing m.

III. PARAMETER EXTRACTION ON ARTIFICIAL DATA—TWO CASE STUDIES

A. Ideal injecting contact and no trap states

In the first case study, we show how the method can be applied to a material containing no trap states, in a device with an ideal injecting contact. For this purpose, we make use of an artificial set of $J(V)$ data points, which have been generated using the ECDM. In order to study the effect of experimental uncertainty on the current measurement, noise at a level of 10% of the current density, and normally distributed on a $\log_{10}(J)$-scale, was added. The data points were obtained using $\sigma = 0.09$ eV, $N_t = 5 \times 10^{27}$ m^{-3}, $V_{bi} = 1.7$ V, and a temperature dependence of the mobility in the limit of zero field and zero carrier density given by

$$\mu_0(T) = \mu_0^* \exp\left[-C\left(\frac{\sigma}{k_B T}\right)^2 \right] \tag{7}$$

with $C = 0.30$, a typical value expected within the ECDM,[15] and with $\mu_0^* = 1 \times 10^{-9}$ m^2/(Vs). The relative dielectric permittivity ε_r was taken equal to 3.2. Using a method for solving the 1D-continuum drift-diffusion equation described in Ref. 8, six sets of $J(V)$ data points were calculated, viz. for organic layer thicknesses equal to 67 and 122 nm and for three temperatures (272, 214, and 170 K). They are shown as symbols in Figure 2.

Before analyzing these artificial data using the parameter extraction method developed in Sec. II, we would first like to give some comments on the data selected. In all case studies presented, the voltage range has been chosen such that both the low-voltage diffusion dominated transport regime and the high-voltage drift dominated regime have been included, in order to create a more rich data set. Furthermore, we note that although actual experimental data sets are often more dense (taken at smaller voltage or current density intervals), the set of 12 data points per curve used already provides an accurate description of its detailed shape, at the noise level assumed. We expect that extending the data set would only be beneficial as long as the experimental errors are truly uncorrelated, so that the accuracy is improved due to the resulting effective data-averaging, and under the condition that the model used is truly appropriate. These criteria will be both met in the case of using artificially generated data, as in this section. However, it is not evident that such an advantage of making use of more measured data points will straightforwardly arise when studying experimentally realistic systems. In such a case, one should also carefully consider other possible contributions to the experimental uncertainty,

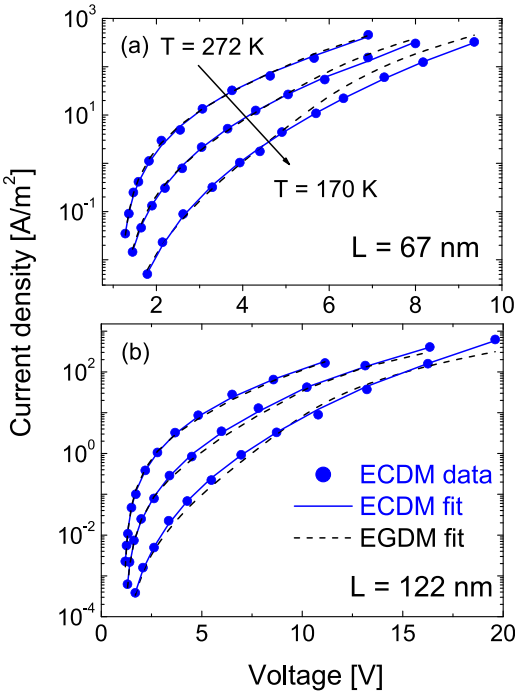

FIG. 2. $J(V, L, T)$ characteristics, generated using the ECDM with 10% noise in J (•), obtained from a fit using the ECDM (solid lines) and obtained from a fit using the EGDM (dashed lines), for an organic layer thickness equal to 67 nm (a) and 122 nm (b) and for a temperature equal to 272, 220, and 170 K. The parameter values used for generating the curves are given in the text.

such as drift, hysteresis, and sample-to-sample variations, as well as the fact that any model used will only describe the current-voltage curves with a certain finite precision. These considerations, as well as the computational effort, should be taken into account when choosing the voltage or current density intervals. The richness of the data set is furthermore strongly enhanced by varying the layer thickness. That makes it possible to make a distinction between injection-related parameters (injection barrier) and the bulk transport parameters. It also facilitates making a distinction between different transport models, as shown in Ref. 16. Finally, by using the temperature variation of the current density, it is possible to more sensitively determine the width and site density characterizing the Gaussian DOS. The strong increase of the current density with temperature reflects the thermally activated nature of the critical hopping processes giving rise to percolative transport, from the low-lying tail states in the Gaussian DOS in which most carriers reside to high-lying states near the top of the Gaussian DOS.[2,6,33]

The solid curves in Figure 2 show the result of a best fit to the data as obtained using the method described above and making use of the ECDM. In order to investigate to what extent it would be possible to make a distinction with the EGDM, a second fit was made to the data assuming the latter model (dashed curves). The figure clearly shows that the fit quality as obtained using the ECDM is significantly higher than as obtained using the EGDM. It is thus indeed possible in this case to make a distinction between both models.

In Figure 3, a more detailed analysis of the fit results is given. Figure 3(a) shows the evolution of the χ^2-value as a function of the iteration number. The ECDM-fits are found

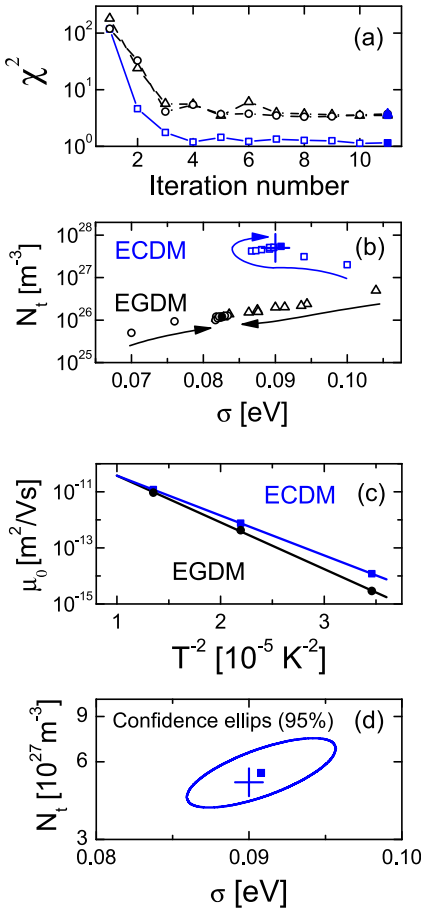

FIG. 3. Results of the ECDM and EGDM analyses presented in Sec. III A. (Un)converged results are indicated by open (filled) symbols. The plus symbols indicate the initial parameter values. (a) Sequences of χ^2-values as obtained using the ECDM (□) and the EGDM (△ and ○), in the latter case resulting from two different starting points. (b) Trajectories in the (σ, N_t)-plane corresponding to the sequences shown in Figure 3(a). (c) Temperature dependence of μ_0 (symbols) and best fits based on Eq. (7) (solid lines). (d) Projection of the full 95% confidence ellipsoid on the (σ, N_t)-plane.

to converge within four iterations to a stable χ^2-value close to 1. The figure also shows the EGDM-results, obtained after starting at two different positions in parameter space (see below). Again, fast convergence is obtained, in this case to $\chi^2 \approx 4$. In Table II, an overview is given of the parameter values obtained from the ECDM fit and of the confidence intervals. The confidence intervals are quite small. Therefore, a symmetric confidence interval has been given for N_t and μ_0 instead of the slightly asymmetric interval, which would follow from considering the logarithms of these parameters as the quantities used in the fitting procedure. A χ^2-test (see Sec. II) yields in these cases $p = 0.1$ and $\sim 2 \times 10^{-17}$, respectively. The former value is consistent with the use of the correct physical model, whereas the latter rather extreme value is consistent with the fact that an incorrect model (the EGDM) has been used. In a more quantitative manner, this thus confirms that it is indeed possible to make a distinction between both models on the basis of an analysis of $J(V)$ curves.

Figure 3(b) shows the sequence of the parameter values σ and N_t obtained. The ECDM-sequence shows that the final parameter values are not necessarily monotonically approached,

TABLE II. Initial and obtained parameter values for the ECDM data sets studied in Secs. III A and III B, analyzed using the ECDM model. A trap DOS, characterized by the parameters $N_{t,trap}$ and E_0 (see text), was only assumed in Sec. III B.

Parameter	Initial	Obtained Section III A	Obtained Section III B
N_t [10^{27} m^{-3}]	5.0	5±1	4.5±1
σ [meV]	90	90±3	89±4
V_{bi} [V]	1.7	1.71±0.01	1.69±0.02
μ_0(272 K) [10^{-11} m^2/(Vs)]	1.2	1.17±0.09	
μ_0(214 K) [10^{-13} m^2/(Vs)]	7.6	8±1	
$N_{t,trap}$ [10^{24} m^{-3}]	2.0		1.6±0.4
E_0 [meV]	103		107±4
μ_0(300 K) [10^{-11} m^2/(Vs)]	2.6		2.5±0.2
μ_0(170 K) [10^{-14} m^2/(Vs)]	1.2		1.2±0.4

but that the final values (solid symbols) obtained are very close to the initial values used (cross). The two EGDM-sequences converge to essentially the same end point, independent of the largely different starting points. The σ-value obtained is only slightly different from the value assumed. However, the site density N_t obtained is approximately a factor 50 smaller than the value assumed. The finding of such a huge difference in the value of the site density obtained makes it possible to discriminate the EGDM and the ECDM using transport measurements, as N_t is usually well-known from independent molecular density measurements, as suggested in Ref. 27.

Figure 3(c) shows that the values of $\mu_0(T)$ as obtained within the EGDM vary linearly (on a log-scale) with $1/T^2$, with a slope parameter C (defined in Eq. (7)), which is approximately 0.42. The slope-parameter is significantly larger than the value of 0.30, which was used to generate the set of ECDM data points (for the values of $\mu_0(T)$ set to calculate the ECDM-based $J(V)$ curves used. However, as such a linear relationship with a larger slope could be consistent with the EGDM,[6,33] it is in this case not possible to use the temperature dependence of $\mu_0(T)$ to make a distinction between both models.

The uncertainties in the parameter values obtained are in a more complete manner given by the joint probability distribution, which (as discussed in Sec. II) may be visualized by giving confidence ellipsoids. Figure 3(d) gives the projection of the five-dimensional 95%-confidence ellipsoid on the (σ, N_t)-plane. The figure reveals a strong correlation between both parameters, corresponding to a correlation coefficient equal to 0.7. The ellipsoid extends in the long direction to the region outside the individual-parameter confidence interval given in the Table, in this five-dimensional case to maximum deviations from the optimal fit value of each of the parameters equal to 3.33 ($= \Delta_5$) times their standard deviation.

From Figure 3(b), it was found that the site density can be used to distinguish both models, as a factor of 50 differences with a quite small uncertainty margin was found. Now the question arises to what extent for any arbitrary (σ, N_t) combination an analysis using an incorrect model gives rise to a significantly different value of N_t. To investigate this, a

single artificial noise-free $J(V)$ curve was generated using both the EGDM and the ECDM at 273 K for 100 nm devices with a built-in voltage of 1.7 V, no barrier at the injecting contact, $N_t = 1 \times 10^{27}$ m^{-3} (ECDM) and $N_t = 5 \times 10^{26}$ m^{-3} (EGDM), for values of σ in the range 0.07 to 0.14 eV. A least-squares fit using the other model shows then how the initial points in either parameter space are projected to points in the other parameter space. The obtained values of V_{bi} and μ_0 were found to be only marginally different from the initial values. Figure 4 gives an overview of the resulting projection in the (N_t, σ)-space. In order to investigate the sensitivity of the projection to the other initial parameters used, the calculations starting from an ECDM-$J(V)$ curve obtained using $\sigma = 0.1$ eV were repeated three times, viz. using $T = 173$ K, $L = 300$ nm, and using a 0.4 eV barrier at the injecting contact. Only very small changes of the end points were found, indicating that the projection shown in Figure 4 is not very sensitive to the temperature, layer thickness, and barrier at the injecting contact used. It can clearly be seen that applying the ECDM to the EGDM-data leads to a substantially higher site density, about a factor of 20, whereas about the same σ-value is obtained. Similarly, applying the EGDM to the ECDM-data leads to a substantially lower site density, about a factor of 10–100. Also, in this case, the σ-values are only slightly different, up to 0.015 eV at most. The observed large effect on N_t is consistent with the results of earlier analyses of experimental data on various materials (PF-TAA,[27] α-NPD,[28] and BAlq[29]), in which a similar substantial difference in site density was found. That made it possible (together with the known experimental site density) to make a distinction between both models.

B. Material with trap states

As a next step, the ability of the method to accurately determine the materials and device parameters from an analysis of current-voltage curves was investigated for a more complex case, with more free parameters, viz. for a material with a realistic small exponential density of trap states. The analysis was applied to an artificial data set consisting of four $J(V)$ curves generated at 300 and 170 K for a layer thickness of 100 and 300 nm using the ECDM. Noise (10% in J) was added to the data to mimic the experimental uncertainty. An ECDM-analysis was used to investigate the effect of this level of noise on the uncertainty of the parameter values obtained. A χ^2-test was found to yield $p = 0.4$, consistent with the use of the correct model to analyze the data.

Table II (last column) contains an overview of the seven parameter values assumed and obtained. The table shows that, using the methodology described in Sec. II, all parameters are found to be equal to the initial values, within the confidence intervals. In order to further analyze the consistency of the approach and the consistency of the obtained parameters, we have investigated the variation of χ^2 as a function of σ, around the optimal point. This was done by carrying out fits to the data while constraining σ and in some cases also some other parameters. The results are shown in Figure 5.

In Figure 5(a), the solid square shows the end-point of the extraction procedure, at which it was regarded as converged. Further iterations only lead to small noisy variations around this end-point. The full curve shows the function $\chi^2(\sigma)$, which is predicted without any other constraint using Eq. (2) on the basis of the calculated derivatives of the $J(V)$ curves in the optimal point. This approach provides a set of

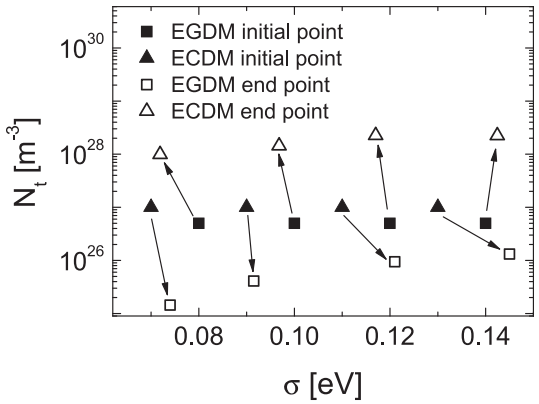

FIG. 4. Fit parameters (open symbols) obtained using the EGDM and the ECDM for $J(V)$ curves generated using the other model and using the initial σ and N_t parameter values indicated by the solid symbols. The calculations were carried out for 100 nm thick devices assuming $T = 273$ K. The other initial parameters are given in the text.

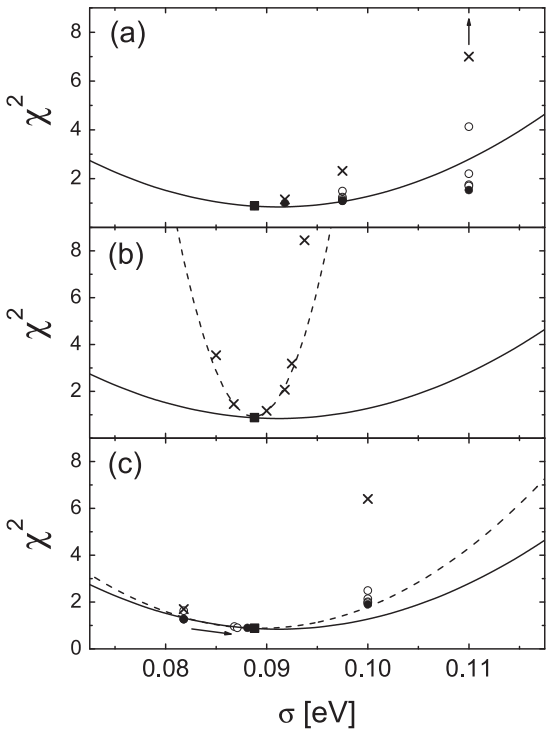

FIG. 5. Effect on the χ^2-value as obtained from the ECDM analysis presented in Sec. III B when constraining some of the parameter values. Solid square: end-point of the extraction procedure. Full (dashed) curves: $\chi^2(\sigma)$-curve around the best fit σ-value as predicted using Eq. (2) without (with) constraints. Crosses: χ^2-values obtained from the actual model calculations using the predicted optimal values (Eq. (2)) of all non-constrained parameters. Solid spheres: χ^2-values, obtained from the re-application of the parameter extraction method while constraining σ and all other parameter values specified. Open spheres: intermediate (non-converged) results. (a) All parameters free, except σ. The arrow indicates that the value of the upper datapoint (cross) at $\sigma = 0.11$ eV is actually far outside the frame of the figure, viz. at $\chi^2 \approx 300$. (b) All parameters constrained, except for the mobility parameters μ_0. (c) All parameters free, except σ and N_t. Arrow: see full text.

predicted optimal values of all other parameters under the constraint of a fixed value of σ. Within the σ-interval shown, a significant increase of χ^2 above the minimum value is expected. In order to test the validity of this prediction, we first calculated the value of χ^2 under the constraint of a fixed value of σ, while taking all other parameter values equal to optimal values at the value of σ selected, as predicted from Eq. (2) (crosses). These explicitly calculated values of χ^2 are found to be larger than the predicted values, with a difference that increases with increasing σ-distance from the optimal point. Subsequently, the parameter extraction procedure was carried out while constraining σ to these fixed values and while leaving all other parameters free. The open and solid spheres show the intermediate and final resulting χ^2 values, respectively. It may be seen that in all cases good convergence was obtained in only a small number of iterations. The final χ^2 values are at every σ value smaller than as predicted. This shows that, in this case, the linearization assumption gives rise to an underestimation of the uncertainty of the parameter values obtained.

Subsequently, we have investigated whether, within the scope of the method, the uncertainty in the parameter values could be improved by reducing the number of free parameters. The dashed curve in Figure 5(b) shows the predicted $\chi^2(\sigma)$ curve as obtained using Eq. (2) when taking all other parameters equal to the values given in Table II, except for the mobility at the two temperatures considered. This curve is found to be in good agreement with the explicitly calculated values of χ^2 as obtained under the same constraints for the predicted optimal values of the two mobilities at the value of σ selected (crosses). From the strongly enhanced curvature of the χ^2-curve, it follows that constraining all other parameters except for the mobilities would give rise to a significant reduction in the uncertainty of σ.

In practice, often the only available additional information on the materials and device parameters, which determine the $J(V)$ curves is the hopping site density N_t. We have, therefore, repeated the analysis for a number of fixed values of σ while taking N_t equal to the initial value (see Table II). All other parameters are left free. Using the same symbols and curve types as above, Figure 5(c) gives the results of such an analysis. The curve which is predicted using Eq. (2) using these constraints (dashed) is found to deviate at $\sigma = 0.10\,\text{eV}$ from the explicitly calculated value that is obtained using values of the parameters predicted with Eq. (2) (cross). That indicates that, at this distance from the assumed set of parameters, the linearization assumption is not anymore very accurate. The curvature of the dashed curve is still larger than that of the unconstrained (full) curve. It thus follows that the optimal value of σ (and of the other parameters) may be determined with a smaller uncertainty than when not constraining any parameter value. Around the optimal point, the $\chi^2(\sigma)$-curve is quite shallow. However, we find that this does not hamper the fast determination of the optimal value of σ from the extraction procedure. If, e.g., after a calculation for $\sigma = 0.082\,\text{eV}$ with a fixed value of N_t subsequently all parameters are left free, the initial σ-value is reproduced, as indicated in Figure 5(c) by the arrow.

For many materials, N_t is expected to be equal to the molecular site density, which may be determined accurately from the density and molecular weight of the material. Recently, support for this picture was obtained from a study of the hopping site density dependence of the mobility for polymers based on a bispirofluorene derivative containing co-polymerized hole-transporting amine units.[9] We, therefore, view constraining N_t as a realistic and practical approach towards extracting the other parameter values with increased accuracy.

IV. APPLICATION TO HOLE AND ELECTRON TRANSPORT IN PF-TAA

A. Hole transport

As a next step, the method is applied to previously published hole-only and electron-only $J(V)$ curves for devices based on a blue-emitting PF-TAA,[8,26,27] and a comparison is made with the uncertainty estimates as obtained in these studies in a much more time-consuming manner by exploring possible solutions on a grid consisting of a large number of points in parameter space surrounding the optimal point. The hole-only devices studied have the structure

$$|\text{glass}\ |\text{ITO}|\ \text{PEDOT:PSS}|\ \text{PF-TAA}\ |100\,\text{nm Pd}|$$

with an indium tin oxide (ITO)/poly(3,4-ethylenedioxythiophene):poly(styrene sulfonic acid) (PEDOT:PSS) anode layer, the PF-TAA light-emitting layer, and a palladium cathode. The structure and functioning of the PF-TAA copolymer have been described in Ref. 8. We employed the measured $J(V)$ curves at 272 and 215 K for device layer thicknesses of 67 and 122 nm, given in this work. Furthermore, we have investigated the experimental uncertainty in the measured current density by repeatedly re-measuring the $J(V)$ characteristics of the same devices at each temperature and layer thickness. A statistical analysis revealed an approximately Gaussian distribution with a standard deviation of about 4% at 273 K. Reanalyzing the $J(V)$ characteristics using the EGDM, including the uncertainty in the measured current-density, led to quick convergence to the same end point, independent of the initial conditions. Within the analysis, all parameter values were treated as identical for each layer thickness, apart from the value of V_{bi}, which is known to show in practice small sample-to-sample variations. The χ^2 value was $\sim$10, which leads to $p = 10^{-75}$. We view these values as an indication that the procedure underestimates the experimental uncertainties, which actually also contain a contribution due to an uncertainty in the layer thickness and measurement temperature. The influence of the latter uncertainties is described in more detail in the Appendix. However, we cannot exclude that the EGDM does not provide a sufficiently accurate description of the transport process, which would also lead to an unacceptably high value of χ^2. The total uncertainty of the parameter values is expressed as a sum of contributions from the covariance matrix analysis, assuming the nominal values of L and T, and a contribution which is due to the experimental uncertainty in L and T. For this case, with five parameters, the Gauss-Newton extraction method requires approximately

10 times less $J(V)$ curve calculations as compared to the previously used "grid approach."[27] Within that approach, χ^2 is calculated on a dense grid of parameter value combinations. Using the Gauss-Newton method significantly reduces the calculation time required for an extraction. The method only requires a linear increase in calculation time with every additional parameter, whereas a power law increase is obtained using the grid approach. The benefit of the extraction method thus increases rapidly with an increasing amount of parameters.

Table III gives an overview of the modelling results and includes a comparison with the results obtained in Ref. 8. It may be seen that within the uncertainty margins, essentially the same parameter values were obtained, *albeit* with a larger and smaller uncertainty margin for the cases of N_t and σ, respectively. This confirms the validity of the earlier results and shows how the Gauss-Newton method can be used as a quick method for extracting the transport parameters and their uncertainties.

In Sec. III A, it was argued that it is in principle possible to make a distinction between the EGDM and the ECDM on the basis of the χ^2-value obtained. However, that would require that the experimental uncertainties are small and well-understood. We find that a re-analysis of the data using the ECDM leads to a fit with a similar χ^2 value as for the EGDM, $\chi^2 \approx 10$, and with an unrealistically large site density. The χ^2-value is, again, larger than the value expected when only random errors in the current density measurement would play a role. The finding of a similar ECDM and EGDM fit quality and essentially the same high ECDM hopping site density was reported previously in Ref. 27. This confirms that, in practice, a distinction between both models is most easily made on the basis of the site densities obtained, if the experimental value of N_t is known. Only a strong reduction of the uncertainties in the experimental values of L and T would, in this case, make it possible to make a distinction on the basis of the fit quality. We find that a different situation arises when considering the Poole-Frenkel model, within which the mobility is given by

$$\mu = \mu_{0,PF}(T)\exp^{-\gamma(T)\sqrt{F}}. \quad (8)$$

Here, γ is an empirical temperature dependent parameter and F the electric field. This model, applied to the hole-only $J(V)$ curves, leads to $\chi^2 \approx 50$. The EGDM (with $\chi^2 \approx 10$) provides thus a significantly better description of the data. The conclusion from this quantitative analysis is consistent with the more qualitative analysis given in Ref. 8.

TABLE III. EGDM parameter values describing the current density in the PF-TAA based hole-only devices discussed in Sec. IV A, as obtained in Ref. 8 and as obtained in this paper. As in Ref. 8, $\epsilon_r = 3.17$ was taken. For the 67 and 122 nm devices, slightly different values of V_{bi} were found in both studies.

Parameter	Ref. 8	This paper
N_t [10^{26} m^{-3}]	6±1	6±3
σ [eV]	0.13±0.01	0.128±0.003
V_{bi}(67 nm) [V]	1.75±0.05	1.77±0.05
V_{bi}(122 nm) [V]	1.95±0.05	1.90±0.03
μ_0(272 K) [10^{-13} m^2/(Vs)]	9±4	7±3
μ_0(215 K) [10^{-16} m^2/(Vs)]	6±4	8±5

B. Electron transport

The extraction of the parameters which determine the transport in electron-only devices is generally more difficult than for hole-only devices due to the presence of additional traps, as shown in Sec. III B. In this subsection, we show how this limits the accuracy with which the transport parameters can be determined by applying the Gauss-Newton method to the dataset presented in Ref. 26, comprising $J(V)$ curves measured for electron-only devices with the structure

|glass| Al |PF-TAA| LiF| Ca |Al|

with 96, 129, and 149 nm PF-TAA layer thicknesses. The 129 nm devices were studied as a function of the temperature in the 193 to 295 K range in 20 K steps (see Ref. 26 for the details), whereas the other two devices were studied at room temperature (295 K). An EGDM based one-dimensional drift-diffusion device model was employed, and an exponential trap DOS is assumed. The model takes into account the presence of a small 0.3 eV barrier at the electron injecting contact. In the model, the image charge effect on the injection barrier is taken into account as described in Ref. 36. We find that this has a minor effect, since only at rather high voltages, a small barrier lowering is found. We note that, as stated in Ref. 26, the injection barrier has an uncertainty of approximately 0.1 eV. Including this uncertainty would contribute to the uncertainty margin of the parameter values extracted. It will be shown that our more restricted study already reveals limitations on the accuracy with which the transport parameters can be obtained using the extraction procedure.

The Gauss-Newton parameter extraction method was applied for a series of fixed values of the width of the density of states, σ, which was varied from 0.05 to 0.13 eV in steps of 0.02 eV. The mobility μ_0 (at all temperatures considered), the hopping site density N_t, the volume density of trap sites $N_{t,trap}$, the width of the exponential trap density of states, E_0 and the built-in voltage V_{bi} were treated as free parameters. Quick convergence was found in all cases. However, as may be seen from Figure 6, in a broad range of σ values (0.05–0.11 eV), the χ^2 obtained were very similar, viz. around 3.5. It follows that, in this case, the χ^2-curve as obtained from this unconstrained fit cannot be used to accurately determine the width of the DOS. Furthermore, the obtained χ^2 values are significantly higher than 1, which would not be expected for a physically fully correct model. Hence, any further analysis using the fit results should be regarded with caution. Nevertheless, the increased χ^2 value found at $\sigma = 0.13$ eV suggests that σ is likely to be smaller than that value.

Figure 7 gives an overview of σ-dependence of the parameter values obtained. Figure 7(a) shows that the obtained hopping site density decreases slightly with increasing σ.

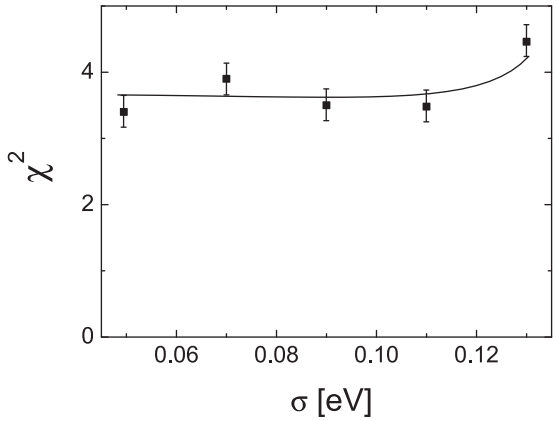

FIG. 6. Obtained best fit χ^2-values as a function of the width of the density of states σ, for the case studied in Sec. IV B. The uncertainty margins of every point and a guide-to-the eye (drawn curve) are shown.

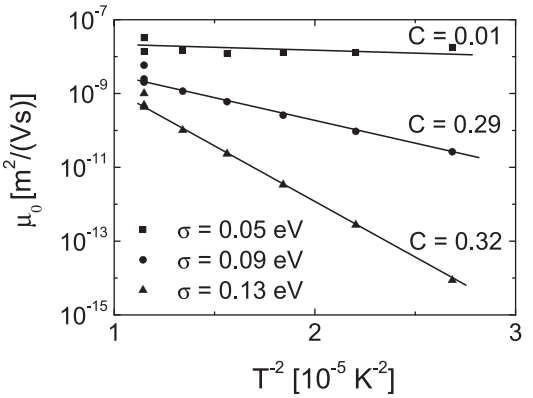

FIG. 8. Obtained best-fit temperature-dependent values of the mobility, μ_0, for three different values of σ (symbols), linear fits to data (lines), and the values of the slope parameters C (defined by Eq. (7)).

However, all N_t values lie in the range $(1.0 \pm 0.5) \times 10^{27}$ m^{-3}, as expected for PF-TAA.[26] Therefore, it is in this case not possible to improve the accuracy of the analysis by making use of a constrained value of N_t. Similarly, no independent experimental information on the trap density, the width of the trap distribution, and the built-in voltage, given in Figures 7(b)–7(d), is available, so that also the σ dependence of these quantities cannot be used to improve the accuracy of the analysis. We remark that the built-in voltage found, in the range 0.5–0.7 V, is close to the value of the compensation voltage of 0.55 V, observed for these devices using photoconductance experiments.[38] Additionally, one could perform electroabsorption or capacitance-voltage measurements to independently judge the accuracy of the value of the built-in voltage obtained.[39] It is interesting to see that a very similar value of the width of the trap distribution, expressed in the figure in terms of the characteristic temperature $T_0 \equiv E_0/k_B$, is obtained

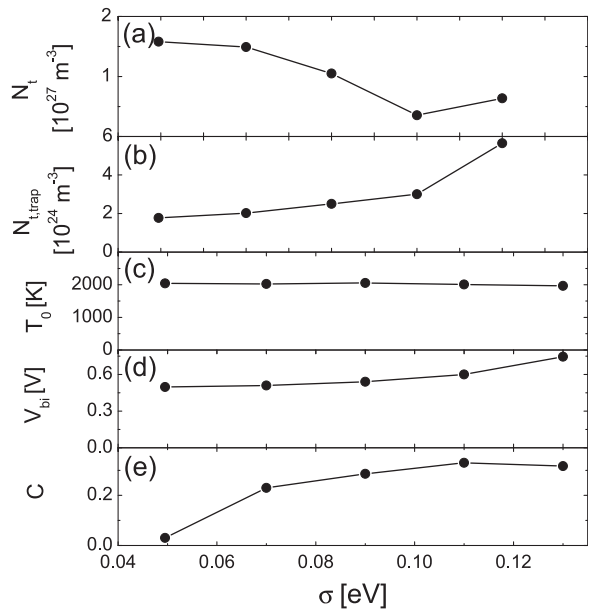

FIG. 7. Obtained best-fit parameters as a function of the width of the density of states, σ, for the case studied in Sec. IV B, for (a) the site density, (b) the trap site density, (c) the trap width, (d) the built-in voltage, and (e) the C parameter, defined by Eq. (7).

for every σ-value studied. This can be understood from the fact that this parameter is strongly determined by the slope of the $J(V)$-curves, when drawn on a log-log scale.[37] Being independent of the other parameters, T_0 can thus be determined with a high accuracy.

Figure 8 shows the temperature dependence of $\mu_0(T)$, for three fixed values values of σ. In all cases, to a good approximation, a $1/T^2$ dependence is found. Such a dependence is expected within the framework of the Gaussian disorder model, with a dimensionless slope (the C-value defined by Eq. (7)) in the range ~0.4 to 0.6 or slightly larger, depending on the details of the model.[6,33,40] Therefore, the obtained value of $C = 0.01$ for $\sigma = 0.05$ eV may be regarded as unphysically small. In Figure 7(e), the variation of the C parameter with σ is shown. Even the values of the C-parameters for $\sigma = 0.09$ eV and 0.13 eV, which are 0.29 and 0.32, respectively, are rather low.

The large values of χ^2 and the somewhat small value of the C-parameter indicate that in this case, with a relatively large number of parameters, either a more refined exploration of the parameter space would be needed, including, e.g., a detailed study of the effects of changing the electron injection barrier or a lateral distribution of barrier heights and the application of independent experimental methods for enriching the data set, or that the development of a refined transport model would be required. We note that, nevertheless, using the model discussed successful modeling of the current density and current efficiency of OLEDs based on PF-TAA was demonstrated.[41] It will be of interest to investigate whether the observed trapping may be better described by assuming a Gaussian trap DOS, as has been proposed recently for a wide range of polymers by Nicolai *et al.*[42] Alternatively, the applicability to polymers of the molecular-scale model leading to a Gaussian DOS with an intrinsic superimposed exponential low-energy tail, presented recently by May *et al.*[23] for the case of small-molecule materials, might be explored. Furthermore, it might be relevant in this case to reconsider the assumption that the transport occurs in between rather localized point sites, instead of more extended conjugated segments. For the system studied, a more accurate extraction of the various transport parameters or a refinement of the transport model would require a richer dataset or additional

specific information about the material or devices studied. For example, Figure 7(a) shows that having prior knowledge about the hopping site density N_t would be useful since it can reduce the uncertainty in the value of σ. For polymer materials such as poly-phenylene-vinylenes (PPVs), for which the value of N_t for HOMO and LUMO states is expected to be very similar, such information can be obtained from a hole-only study.[35] However, such an approach cannot be used for the case of PF-TAA, which contains hole-transporting units, so that the hopping site density for electrons is different from that for the holes.

V. SUMMARY AND CONCLUSIONS

A Gauss-Newton extraction method was developed for quickly deducing the materials and device parameters, which determine the mobility in an organic material from the $J(V)$ characteristics. We have studied the accuracy and limitations of its application to realistic organic semiconductor devices. For selected cases, the experimental uncertainties were quantified using a statistical analysis of the experiments. The parameter uncertainties and their correlations were quantified using co-variance matrices.

Applying the method to artificially generated ECDM hole transport data with additional noise using both the EGDM and the ECDM showed fast convergence to a unique point in the parameter space. Making a distinction between both models was found to be possible by comparing the hopping site density as obtained from the analysis and the experimental value. When applied to generated electron transport data with additional noise, the presence of additional parameters which describe the shape of the trap DOS was found to make the extraction more difficult. As more parameters are presented, the obtained uncertainty margins are larger. Reducing the uncertainty margins was shown to be possible by constraining the hopping site density to its experimental value.

The method has also been applied to experimental data. For the case of the hole transport $J(V)$-characteristics of the blue-emitting polymer PF-TAA, convergence to essentially the same parameter values as obtained in a previous study[8] was found, but in a much quicker manner. For this case, the influence of the experimental uncertainty in the organic layer thickness and temperature on the determined parameters was taken into account. A comparison with the empirical PF model showed that a significantly higher fit quality is obtained when using the EGDM. A quantitative comparison between different mobility models can thus be made using the method. For the electron transport characteristics of PF-TAA, the application of the extraction method under the assumption that the mobility may be described within the framework of the EGDM, with a small exponential trap DOS superimposed on the Gaussian DOS, revealed limitations. A similar fit quality was obtained for a rather wide range of parameter value combinations. To a certain extent, constraining the parameter set is possible by comparing the temperature dependence of the mobility in the Boltzmann limit as deduced from the simulations with the temperature dependence as expected within the framework of the EGDM. However, constraining the parameter set further would require carrying out additional experiments. The method can thus be used to determine quickly whether carrying out additional experiments which enrich the available data set is needed. Subsequently, it may be used in a "design of experiment" approach within which the accuracy enhancement resulting from parameter extraction under various constraints is calculated, from which it then may be determined which experiment can most efficiently be added to make more unique extraction possible.

APPENDIX: EXPERIMENTAL UNCERTAINTY

Within the Gauss-Newton parameter extraction method, the experimental uncertainty in the observable is assumed to be normally distributed. In order to verify this assumption and to quantify the experimental uncertainty for a typical experimental case, the current-density was measured multiple times for a hole-only device of the type studied in Sec. IV A at a fixed voltage and temperature. Figure 9 shows the result of a statistical analysis of the data. It can be seen that the data are indeed fairly well described by a normal distribution.

Figure 10 shows the voltage dependence of the standard deviation of $\log_{10}(J)$, measured at two temperatures. At room temperature (295 K), no active temperature control is used. This leads to a small experimental uncertainty, of about 0.5% to 2% for voltages above 2 V. This percentage is calculated using $(10^{\alpha}\text{-}1) \times 100\%$, where α is the standard deviation in $\log_{10}(J)$, as obtained from Figure 10. At 273 K, an active temperature control is used. This leads in our setup to a higher uncertainty, up to 4% above 2 V. The peak in the uncertainty in the lower voltage regime corresponds to the steep onset of the current-density, which occurs at a temperature-dependent voltage, which is significantly smaller than the built-in voltage due to charge-carrier diffusion.[39] The parameter extraction results presented were based only on $J(V)$-points well above V_{bi}. In particular, for the temperature and layer thickness dependent set of $J(V)$ curves considered in Sec. IV A, the experimental uncertainty was determined for every experiment. This gives a balanced weight to every measured current-density.

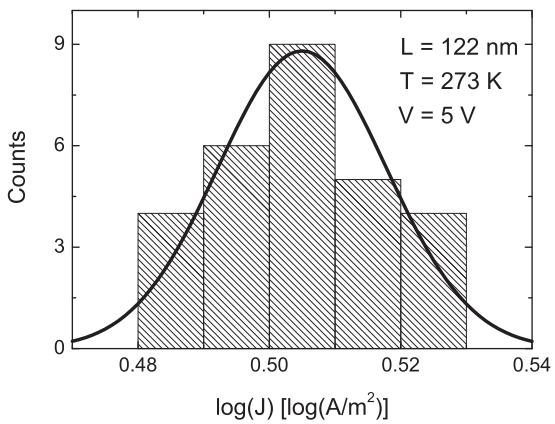

FIG. 9. Histogram of the measured current density at 273 K and at 5 V for a hole-only PF-TAA based device with a layer thickness of 122 nm, as discussed in Sec. IV A. The solid line shows the best-fit normal distribution.

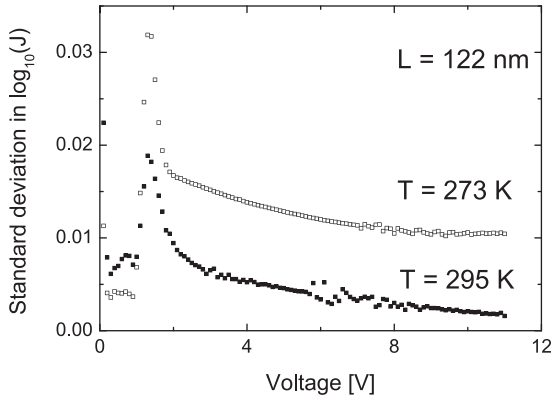

FIG. 10. Voltage dependence of the standard deviation of the measured current density for two temperatures (295 K and 273 K) in a PF-TAA based hole-only device with a layer thickness of 122 nm, as discussed in Sec. IV A.

The uncertainty in the obtained parameter values is in practice also influenced by a non-random contribution due to errors in the layer thickness (ΔL) and in the (average) measurement temperature (ΔT). Both uncertainties lead to a (non-random) shift of the $J(V)$ curves. The resulting uncertainty in the parameter values can be obtained by making use of a Taylor expansion of the function F_i (defined in Eq. (1)) around the optimal set of parameters, i.e., by writing

$$F_i(\Delta L, \Delta T) = F_i(0,0) + \frac{\partial F_i}{\partial L}\Delta L + \frac{\partial F_i}{\partial T}\Delta T \qquad \text{(A1)}$$

and by subsequently minimizing the corresponding χ^2-value

$$\chi^2(\Delta L, \Delta T) = \min_{\Delta P_j}\left\{\frac{1}{n}\sum_{i=1}^{n}[F_i(\Delta L, \Delta T) + \frac{\partial F_i}{\partial P_j}\Delta P_j]^2\right\}, \qquad \text{(A2)}$$

in order to obtain the optimal change ΔP of each of the parameters (j). This optimal change can be used as a measure for the uncertainty in every parameter due to the mentioned non-random uncertainties. For the case studied in Sec. IV A, $\Delta L = \pm 2$ nm and $\Delta T = \pm 2$ K were taken to obtain the confidence intervals given in Table III.

[1]V. Coropceanu, J. Cornil, D. A. da Silva Filho, Y. Olivier, R. Silbey, and J. L. Bredas, Chem. Rev. **107**, 926 (2007).
[2]H. Bässler and A. Köhler, Top. Curr. Chem. **312**, 1–65 (2012).
[3]M. C. J. M. Vissenberg and M. Matters, Phys. Rev. B **57**, 12964 (1998).
[4]C. Tanase, E. J. Meijer, P. W. M. Blom, and D. M. de Leeuw, Phys. Rev. Lett. **91**, 216601 (2003).
[5]C. Tanase, P. W. M. Blom, D. M. de Leeuw, and E. J. Meijer, Phys. Status Solidi A **201**, 1236 (2004).
[6]W. F. Pasveer, J. Cottaar, C. Tanase, R. Coehoorn, P. A. Bobbert, and P. W. M. Blom, Phys. Rev. Lett. **94**, 206601 (2005).
[7]R. Coehoorn, W. F. Pasveer, P. A. Bobbert, and M. A. J. Michels, Phys. Rev. B **72**, 155206 (2005).
[8]S. L. M. van Mensfoort, S. I. E. Vulto, R. A. J. Janssen, and R. Coehoorn, Phys. Rev. B **78**, 085208 (2008).
[9]H. T. Nicolai, A. J. Hof, M. Lu, P. W. M. Blom, R. J. de Vries, and R. Coehoorn, Appl. Phys. Lett. **99**, 203303 (2011).
[10]Z. G. Yu, D. L. Smith, A. Saxena, R. L. Martin, and A. R. Bishop, Phys. Rev. B **63**, 085202 (2001).
[11]S. D. Baranovskii, I. P. Zvyagin, H. Cordes, S. Yamasaki, and P. Thomas, Phys. Status Solidi B **230**, 281 (2002).
[12]R. Schmegel, Phys. Rev. B **66**, 235206 (2002).
[13]V. I. Arkhipov, P. Heremans, E. V. Emelianova, G. J. Adriaenssens, and H. Bässler, J. Phys.: Condens. Matter **14**, 9899 (2002).
[14]S. Shaked, S. Tal, Y. Roichman, A. Razin, S. Xiao, Y. Eichen, and N. Tessler, Adv. Mater. **15**, 913 (2003); Y. Roichman, Y. Preezant, and N. Tessler, Phys. Status Solidi A **201**, 1246 (2004).
[15]M. Bouhassoune, S. L. M. van Mensfoort, P. A. Bobbert, and R. Coehoorn, Org. Electron. **10**, 437 (2009).
[16]P. W. M. Blom, C. Tanase, D. M. de Leeuw, and R. Coehoorn, Appl. Phys. Lett. **86**, 092105 (2005).
[17]J. Staudigel, M. Stossel, F. Steuber, and J. Simmerer, J. Appl. Phys. **86**, 3895 (1999).
[18]P. W. M. Blom and M. C. J. M. Vissenberg, Mater. Sci. Eng. **27**, 53–94 (2000).
[19]J. J. Kwiatkowski, J. Nelson, H. Li, J. L. Bredas, W. Wenzel, and C. Lennartz, Phys. Chem. Chem. Phys. **10**, 1852 (2008).
[20]Y. Nagata and C. Lennartz, J. Chem. Phys. **129**, 034709 (2008).
[21]A. Lukyanov and D. Andrienko, Phys. Rev. B **82**, 193202 (2010).
[22]V. Rühle, A. Lukyanov, F. May, M. Schrader, Th. Vehoff, J. Kirkpatrick, B. Baumeier, and D. Andrienko, J. Chem. Theory Comput. **7**, 3335 (2011).
[23]F. May, B. Baumeier, C. Lennartz, and D. Andrienko, Phys. Rev. Lett. **109**, 136401 (2012).
[24]J. C. Blakesley, H. S. Clubb, and N. C. Greenham, Phys. Rev. B **81**, 045210 (2010).
[25]J. C. Blakesley and N. C. Greenham, J. Appl. Phys. **106**, 034507 (2009).
[26]S. L. M. van Mensfoort, J. Billen, S. I. E. Vulto, R. A. J. Janssen, and R. Coehoorn, Phys. Rev. B **80**, 033202 (2009).
[27]R. J. de Vries, S. L. M. van Mensfoort, V. Shabro, S. I. E. Vulto, R. A. J. Janssen, and R. Coehoorn, Appl. Phys. Lett. **94**, 163307 (2009).
[28]S. L. M. van Mensfoort, V. Shabro, R. J. de Vries, R. A. J. Janssen, and R. Coehoorn, J. Appl. Phys. **107**, 113710 (2010).
[29]S. L. M. van Mensfoort, R. J. de Vries, V. Shabro, H. P. Loebl, R. A. J. Janssen, and R. Coehoorn, Org. Electron. **11**, 1408–1413 (2010).
[30]I. Bauer, H. G. Bock, S. Korkel, and J. P. Schlodel, J. Comput. Appl. Math. **120**, 1–25 (2000).
[31]H. G. Bock, E. Kostina, and J. P. Schlodel, GAMM-Mitt. **30**(2), 376–408 (2007).
[32]R. C. Aster, B. Borchers, and C. H. Thurber, *Parameter Estimation and Inverse Problems* (Elsevier Academic Press, Oxford, 2005).
[33]J. Cottaar, L. J. A. Koster, R. Coehoorn, and P. A. Bobbert, Phys. Rev. Lett. **107**, 136601 (2011).
[34]M. M. Mandoc, B. de Boer, and P. W. M. Blom, Phys. Rev. B **73**, 155205 (2006).
[35]M. M. Mandoc, B. de Boer, G. Paasch, and P. W. M. Blom, Phys. Rev. B **75**, 193202 (2007).
[36]P. R. Emtage and J. J. O'Dwyer, Phys. Rev. Lett. **16**, 356 (1966).
[37]P. Mark and W. Helfrich, J. Appl. Phys. **33**, 205 (1962).
[38]J. Billen (unpublished).
[39]R. J. de Vries, S. L. M. van Mensfoort, R. A. J. Janssen, and R. Coehoorn, Phys. Rev. B **81**, 125203 (2010).
[40]H. Bässler, Phys. Status Solidi B **175**, 15 (1993).
[41]S. L. M. van Mensfoort, J. Billen, M. Carvelli, S. I. E. Vulto, R. A. J. Janssen, and R. Coehoorn, J. Appl. Phys. **109**, 064502 (2011).
[42]H. T. Nicolai, M. Kuik. G. A. H. Wetzelaer, B. de Boer, C. Campbell, C. Risko, J. L. Bredas, and P. W. M. Blom, Nature Mater. **11**, 882 (2012).